

Growth features of micro- and nanocrystalline diamond films on rotating high-aspect substrates

© E.E. Ashkinazi,¹ S.V. Fedorov,² A.K. Martyanov,¹ A.P. Bolshakov,¹ A.F. Popovich,^{1,3} D.N. Sovyk,¹ A.A. Khomich,³ A.P. Litvinov,² V.G. Ralchenko,¹ S.N. Grigoriev,² V.I. Konov¹

¹ Prokhorov Institute of General Physics, Russian Academy of Sciences, 119991 Moscow, Russia

² Moscow State Technological University STANKIN, 127055 Moscow, Russia

³ Fryazino Branch, Kotelnikov Institute of Radio Engineering and Electronics, Russian Academy of Sciences, 141190 Fryazino, Moscow oblast, Russia

e-mail: jane50@list.ru, art.martyanov@gmail.com, sedovvadim@yandex.ru, lex78@mail.ru, bolshak3@yandex.ru, sovyk@inbox.ru, high-low@yandex.ru, dodeskoden@gmail.com, vg_ralchenko@mail.ru, yurov6591@gmail.com, vity.konov@gmail.com, s.grigoriev@stankin.ru, sv.fedorov62@gmail.com, mrartem.litvinov35801@mail.ru, antares-610@yandex.ru, lex78@mail.ru

Received July 15, 2024

Revised September 9, 2024

Accepted September 10, 2024

As a result of E-field modeling (COMSOL Multiphysical), the functions of the main conducting platform of the microwave reactor were expanded by combining it with a ring-shaped evanescent waveguide that ensures substrate rotation. In this geometry, twelve-layer micro- and nanocrystalline diamond films were deposited on a four-tooth end mill Ø12 mm made of VK-6 alloy (WC+6%Co). The temperature regime of uniform heating of the milling cutter during rotation was determined. The structure, chemical and phase composition of the substrate and the synthesized coating were studied using scanning electron microscopy, X-ray fluorescence analysis and Raman spectroscopy in areas equidistant from the end of the cutter with a step of 5 mm over a length of 25 mm. The proposed geometry of the microwave path of the reactor ensured a favorable concentration of the E-field and uniformity of the temperature in the substrate area. Data on grain sizes and line intensities of diamond and ordered graphite demonstrate both uniformity of the diamond film thickness and an increase in the proportion of microcrystalline diamond compared to nanocrystalline diamond with distance from the end. It is shown that the coating at all points is under elastic compressive stresses increasing from the cutter tip from 0.7 GPa at the end to 1.2 GPa at a distance of 30 mm, reaching a maximum value of 3.1 GPa at a distance of 20 mm.

Keywords: microwave plasma reactor, polycrystalline diamond, chemical vapor deposition of diamond.

DOI: 10.61011/TP.2024.12.60433.233-24

Introduction

Great progress achieved in the diamonds synthesis in 1980 [1] demonstrated a successful deposition of diamond films on the non-diamond substrates by method of chemical vapor-phase deposition (CVD) with a hot filament (HF) at a rate of 0.8–1.5 μm/h. In 1990 [2] the first non-diamond films were fabricated by method of microwave plasma-chemical vapor-phase deposition (MP CVD), and no later than in 2009 using MP CVD method with CVD for diamonds synthesis at a pressure of 300 kPa [3] the record rate of 165 μm/h was reached, which in 2010 was near 250 μm/h [4]. Such rapid progress has also been made with regard to the diamond films quality [5–10].

This material has gained so much interest because of a large number of applications in the aerospace and defense industries, in particular for wear-resistant tools for highly efficient processing of materials. Further expansion of high-quality diamond coatings fabrication using CVD method and on large areas remains the most important prerequisite for their industrial application. In this regard,

the performance of a plasma reactor for specific substrate sizes is of particular importance. Currently, only chemical vapor-phase deposition processes using microwave plasma with a resonant cavity system, provide high performance due to a sufficient amount of atomic hydrogen [11].

As is known, with a large deposition surface, it is necessary to create plasma with a high power density under a strong electric field in the resonant cavity zone. This can be achieved only with effective UHF communication from the source to the substrate. In some cases, an inconsistent plasma load may cause disturbance of the cavity at a very high reflected fraction of the input power [12], and such a discrepancy can lead to pronounced heating and even burning of the walls of the reactor waveguide [5,13]. The aspect ratio of a substrate (the ratio of critical dimensions), which determines its shape, also indirectly affects the geometry of the structural elements of waveguides in CVD plasma reactors for depositing the mono- and polycrystalline diamond films [5,13–16]. This is true for both, the flat-surface (2D) substrates as wafers [17], and to spatial (3D) shapes [16].

Formation of a microwave plasma is sensitive to the geometry of the substrate due to the edge effect, since plasma is concentrated in areas of electric field distortion, especially at the edge of an extensively protruding part, thus causing a non-uniform deposition of the diamond film. The detrimental effect of local microwave field on the temperature rise is aggravated by an increase in the aspect ratio of the substrate [15,18]. Carbide drills and cutters here may serve as an example. Temperature uniformity becomes a critical condition determining the possibility of successful growth of a diamond film on high-dimensional substrates. In the study [19] an original design of an evanescent waveguide (EW) was proposed, which makes it possible to implement the CVD deposition mode, eliminating direct heating of low-dimensional (with a small height-to-diameter ratio) substrates in a microwave plasma reactor. Due to transition to indirect heating, mainly from plasma radiation, the edge effect was significantly reduced, which provided protection of the substrates from overheating [20]. At the same time, the inconsistency in the dimensions of the substrate and the conducting platform provided a great potential for effectively using the platform area if grown on a high-dimensional substrate.

In papers [22,23] an original design of a substrate holder was suggested, making it possible to provide a uniform deposition, excluding direct heating of low-dimensional substrates in a microwave plasma reactor. The transition to indirect heating in the ethereal region of plasma dramatically reduced the edge effect and protected the substrates from overheating, resulting in coatings with uniform morphology both, in the central region and on the periphery, which is consistent with computations of plasma power density in the evanescent waveguide [21,22] using optical emission spectroscopy (OES).

The synthesis of MP CVD diamond coatings on high-dimensional substrates is also of scientific and practical interest in the field of implantology, as it deals with improvement of biocompatibility and extension of service life of implants for fracture healing, joint replacement and bone replacement. Many of the aforesaid implants in terms of geometry represent the solids of revolution [23–25].

Earlier it was reported about the study of a micro-nanocrystalline diamond film grown on a high-dimensional model from a calibrated KFM-39 alloy bar (Konrad Micro Drill 128 (Kulmbach, Germany)) in microwave plasma [26], however, insufficient attention was paid to modeling of E-field of UHF reactor resonator system (2.45 GHz) for conducting a stable process of plasma activation and growth, as well as to modeling the cutter heating to obtain the desired morphology, topography and texture on the cutting surface, formed directly on a carbide tool of complex shape during rotation. In this paper, an in-depth study of these issues was conducted in order to better understand the self-consistent excitation and steady burning of plasma at reduced UHF power and to clarify the role of the temperature effect of CVD growth on structural changes

in micro- and nanocrystalline (MCD/NCD) diamond films on the cutting edges of WC–6%Co carbide cutter.

1. Materials and methods

Preparation and growth on high-dimensional substrates were performed based on a schematic diagram for fabrication of diamond films on WC–Co [20] alloy. The controlled surface of the milling cutter was chemically etched with Murakami and Caro reagents to prevent cobalt diffusion at the temperature of coating deposition. A barrier layer of tungsten with a thickness of 600 nm between the substrate and the diamond film was deposited by method of magnetron sputtering. Figure 1 illustrates the photo of the cutting edge of D12CH0.25x12s12x75 Z4RR cutter before CVD growth after cobalt etching with Murakami and Caro reagents and after deposition of W and MP CVD growth in a mixture of CH₄/H₂ gases, as well as the image of REM microstructure after preliminary treatment.

Etching was performed in an ultrasonic bath in a cylindrical plastic container in a 70 ml reagent mixture at a temperature of 20–29°C. For this, the sample was dipped in the center to the very bottom, where the ultrasound intensity is higher and the etching solution is better mixed. Each time the temperature gradually increased from 20 to 29°C. Etching time in Murakami reagent — 12 min, in Caro reagent — 90 s. X-ray fluorescence (RFIA) analysis was performed by exciting the energy dispersion spectra of characteristic X-ray radiation at an accelerating voltage at the cathode of 18 kV, the spot area for analysis was 60–200 μm². Concentration of basic elements in WC+6%Co carbide in atomic percentage according to RFIA on the energy-dispersive spectrometer „X-MAX“ („Oxford Instruments“) is given in Table 1.

As can be seen, during 12 min of etching in Murakami mixture and during 1.5 min of etching in Caro mixture the near-surface concentration of cobalt in BK-6 sample (№ 2) decreased 20-fold down to 0.25 at.%. Chemical composition analysis both on the cutting edge and on the top of the milling cutter showed similar results.

2. Results and discussion

2.1. Modeling of E-field of resonator system of a UHF reactor

Initially, when modeling E-field of the resonator system of UHF reactor with a high-dimensional UHF substrate, the plasma reactor contained an axisymmetric sealed working chamber [12]. A flat platform was installed inside the chamber, coaxially with it, forming a radial microwave waveguide with the inner end surface of the working chamber. The central part of the waveguide is ended with a resonant cavity. The microwave energy source is connected to the platform and the working chamber by a coaxial cone-shaped waveguide, the base of the inner cone

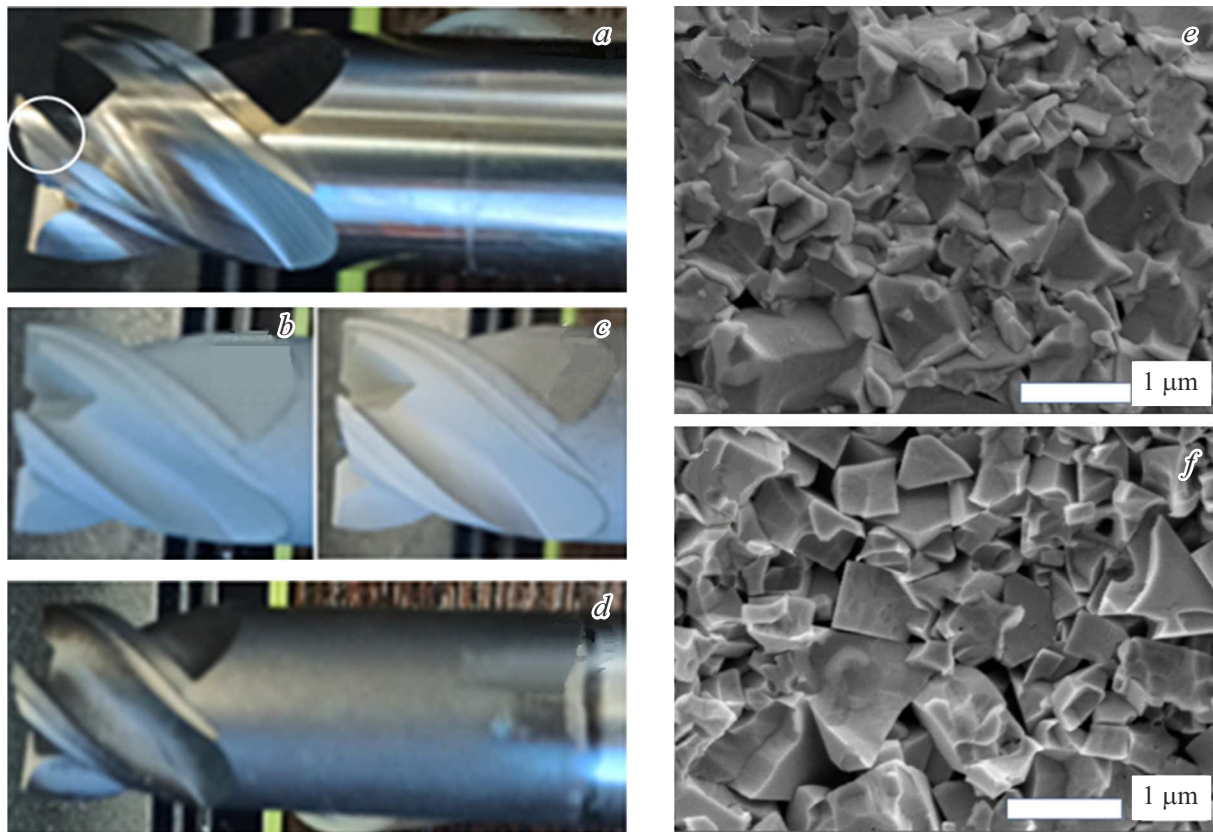


Figure 1. General view of the cutter edge surface (*a*) before the film growing by CVD method (the circle indicates the region studied using methods of raster electron microscopy (REM) and X-ray fluorescence analysis (RFIA)); *b* — after cobalt etching; *c* — after tungsten deposition; *d* — after MP CVD growth. The images of REM microstructure after etching (*e*) and tungsten deposition (*f*).

Table 1. Concentration of carbon, tungsten, cobalt and oxygen in WC+6%Co alloy according to RFIA data, energy-dispersive spectrometer „X-MAX“ („Oxford Instruments“)

Sample of WC+6%Co, concentration of elements, at.%	Concentration carbon, at.%	Concentration tungsten, at.%	Concentration cobalt, at.%	Concentration oxygen, at.%
Before etching	62.17	20.09	5.11	12.63
After etching	76.56	16.98	0.25	6.2

of the waveguide is connected to the platform, while the base of the outer cone (in a common plane) with the base of the inner cone is attached to the chamber's cylindrical wall (Fig. 2, *a*). In general, the geometric proportions of a cone-shaped waveguide correspond to the ratio

$$\ln(\operatorname{tg} \alpha / \operatorname{tg} \beta) = \ln A / B = H / B, \quad (1)$$

where α and β — the angles of inner and outer cones with a common vertex, A — inner radius of cylindrical part of the chamber, B — platform radius, H — distance from the platform to the interior surface of the working chamber. Calculations of the E-field for the chamber of the ARDIS-100 reactor with a modified resonator geometry by introducing an EW allowed us to simulate a self-consistent

resonance in the region of plasma excitation with a EW without a substrate and E-field in the resonant zone with a high-dimensional substrate. In the first case, the field concentration is released in the substrate area from the passive side of plasma emission. The reverse displacement of the field in this case can lead to burnout of coaxial waveguide. The mentioned cases are given in Fig. 2, *a, b*. Computations of E-field for the chamber of ARDIS-100 reactor with the resonator geometry modified by increasing the radius of the conducting platform made it possible to simulate a self-consistent resonance in plasma excitation region without a substrate and E-field in the resonant zone with the introduction of a substrate. In contrast to the previously considered case, the field concentration in the

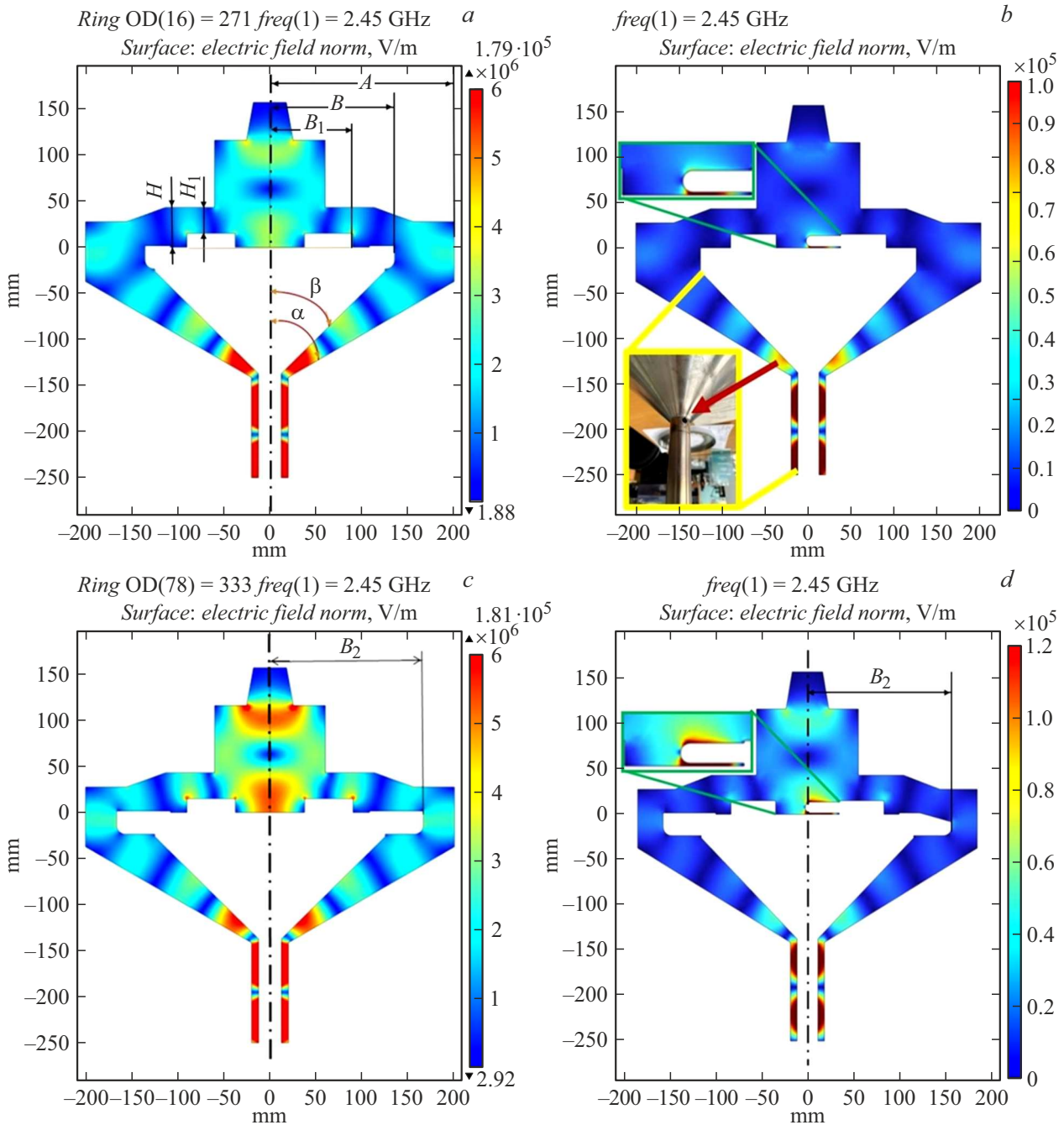


Figure 2. Computations of E-field for the chamber of ARDIS-100 reactor with modified resonator geometry: *a* — self-consistent resonance in the region of plasma excitation with an EW without a substrate; *b* — E-field in resonance zone with high-dimensional substrate; upper insert window shows the field concentration in the substrate area on passive side of plasma emission; *c* — computations of E-field for chamber of ARDIS-100 reactor with the resonant cavity geometry modified by increasing the radius of conducting platform, self-consistent resonance in the area of plasma excitation without a substrate; *d* — E-field in the resonance zone with a substrate, the insert window illustrates the field concentration in the substrate area on the passive side of plasma emission.

substrate region (Fig. 2, *d*, insert) moves to the active side of plasma emission and surrounds the milling cutter along the perimeter.

Designations taking into account the introduced changes are given in Fig. 2, *a, c, d*, where B_1 — the rated radius of EW; B_2 — rated radius of the major conducting

platform; H_1 — distance from EW to the interior surface of the working chamber. As can be seen, in order to ensure a self-consistent resonance when a h high EW is introduced in plasma excitation region, which leads to lower distance from the EW to the working chamber inner surface, and provided condition (1) is met, it is

necessary to match the dimensions of UHF reactor and the conducting platform (B_2). The matching radius of the conducting platform (B_2) was confirmed experimentally by monitoring the heating temperature during growth on a high-dimensional WC+6%Co milling cutter and subsequent investigation of MCD/NCD microstructure of the diamond film.

2.2. Modeling WC+6%Co cutter heating in the UHF-reactor during CVD-deposition of the diamond coating with rotation

Earlier it was reported about the study of a micro-nanocrystalline diamond film grown on a high-dimensional model from a calibrated KFM-39 bar in microwave plasma [26]. In this paper, the heating of a WC-6%Co carbide end cutter was simulated to evaluate the temperature effect of plasma heating on structural changes in MCD/NCD diamond film deposited on the cutting edges of the milling cutter and its chip removal grooves.

The modeling was carried out in ANSYS program with the model breakdown into finite elements. The model itself if a four-teeth end milling cutter ($\varnothing 12$ mm) inserted into a molybdenum holder simulating the EW which protrudes $h = 15$ mm above the conducting platform. To insert and orient the deposited part of the cutter the EW has a $d = 13.5$ mm hole, matched with the cutter diameter. The diameter of hole in EW (molybdenum ring) was taken equal $\sim \lambda/2$ and $2/3\lambda$ (52 and 75 mm respectively). The heating of the milling cutter in the diamond deposition mode is modeled using a surface heater located above the model with a bottom surface temperature of 1100–1250°C. At the first stage, a preliminary computation was carried out to select the heater temperature, at the second stage, the cutter heating was simulated when rotating around its axis in 10° increments, and the temperature of the cutting edge and the chip removal groove were monitored as the most important elements for reliable operation of the milling cutter.

Calculations of thermal field of the milling cutter heating during diamond deposition included a computational model of the holder and the cutter, a cross-section of the thermal field in the cutter body and in its holder, and a model of the milling cutter heating with rotation (Fig. 3). The inserts illustrate the heating of sections most important for reliable operation of the milling cutter, the temperature of the cutting edge and the chip removal groove.

The temperature of the heater which simulates the cutter heating from plasma ball during diamond growth, was assumed to be 1165°C. Further computations were performed with this temperature. The temperature distribution in the molybdenum ring and the milling cutter is shown in Fig. 3, *a*. Heat transfer between objects included radiative heating of surfaces from the lower surface of a heater with a temperature of 1150–1250°C, as well as thermal conductivity in gases and solids. The model was cooled by maintaining a constant temperature of the base

bottom surface, equal to 22°C. A preliminary computation was carried out to select the heater temperature at which maximum temperature of the milling cutter would be equal to 800°C, optimal for the growth of the diamond coating. Fig. 3. illustrates the results of thermal field computations for the chamber of ARDIS-100 reactor, including heater temperature computation depending on the required substrate temperature, cutting edge maximum heating versus growth temperature and the chip removal groove maximum heating versus minimum temperature (shown in the insert window), the uniform heating temperature of the milling cutter surface and the heater profile.

The results of the temperature computation, including a graph for calculating the heater temperature depending on the required substrate temperature, the curves of the cutting edge maximum heating versus growth temperature, as well as the curve of the chip removal groove maximum heating versus minimum temperature are shown in Fig. 4. In our simulation, the convergence criterion was considered to be a change in the model parameters after each iteration by no more than 0.1%.

After that the cutter heating was simulated when rotating around its axis with an increment of 10° (Fig. 4, *b, c*). It can be seen from the graphs that when the milling cutter rotates, the maximum and minimum temperatures of the cutter working surfaces differ by no more than 60–80°C. Presumably, this is due to the smaller cross-sectional area of the cutting part of the milling cutter compared to the cylindrical model, as well as the complex profile when the milling cutter tooth periodically approaches the heater.

2.3. Linear measurements of the cutting edge after sharpening. Defining the cutting edge radius.

The radius of the cutting edge was measured on a milling cutter in the state of delivery (uncoated), after etching with Murakami and Caro reagents, with a barrier tungsten (W) coating and after the growth of CVD diamond film. The radii of the cutting edge were measured at a distance 4–5 mm from the cutter side. The cutters scanning and further measurements of the cutting edge radii were carried out using 3D-scanner MikroCAD Premium. In order to obtain a clear image of the measured area, the milling cutter was pre-cleaned in an ultrasonic bath in propanol, after which 3D-scanning of the cutting edge surface was performed. After the scanning procedure, the radii of the cutting edges were measured. Diagrams of measuring the cutting edge radii of WC+6%Co cutter are given in Table 2 and in Fig. 5.

2.4. Results of Raman scattering spectroscopy

Graphical representation of RS MP CVD spectroscopy of MCD/NCD film on the cutter, including spectra of the diamond film on WC+6%Co alloy depending on the

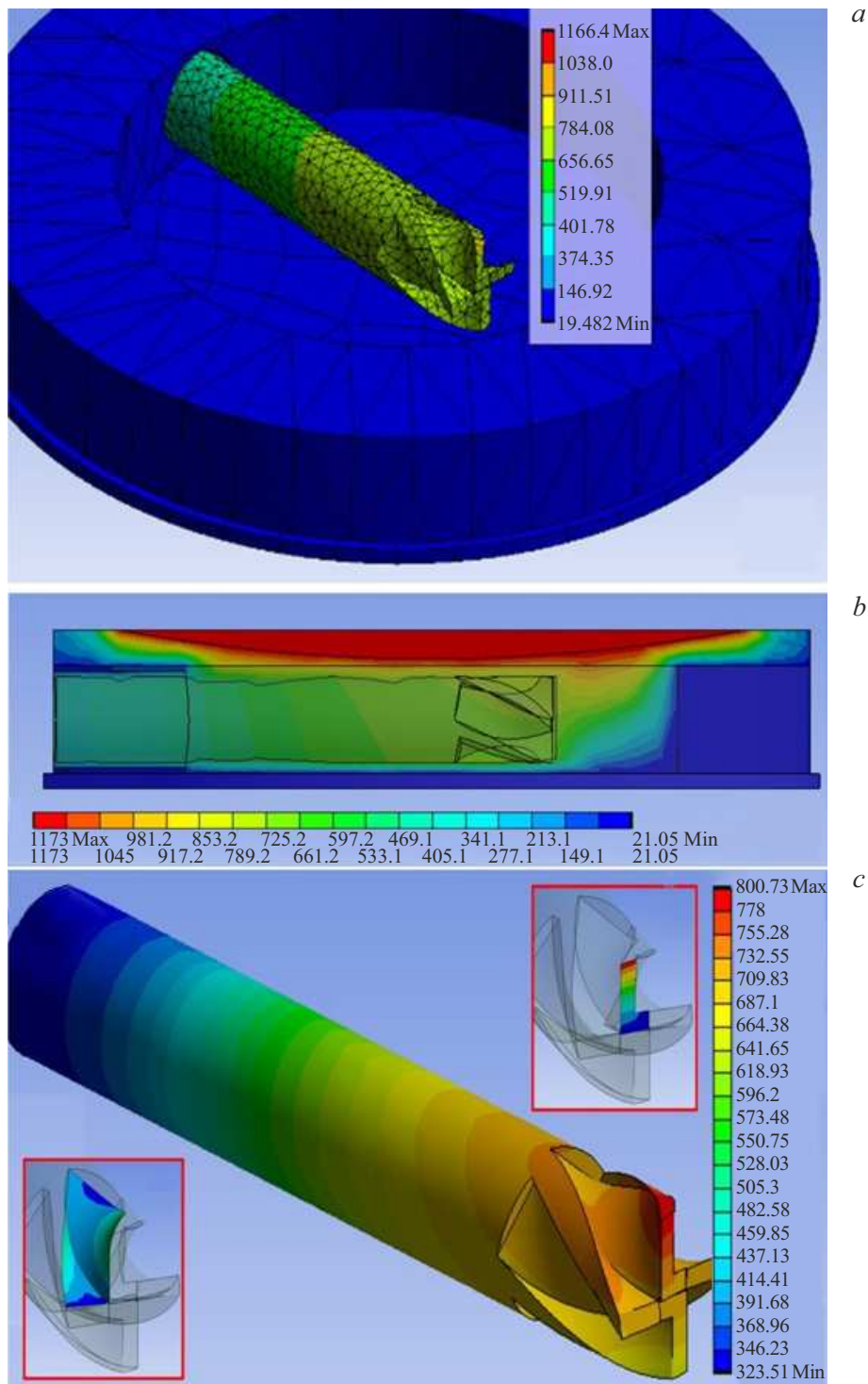


Figure 3. Computations of the cutter heating thermal field during diamond deposition: *a* — computational model of the holder and cutter; *b* — cross-section of thermal field in the cutter body and in its holder; *c* — model of heated cutter with rotation around its axis with an increment of 10° . Insert windows in Fig. 3, *c* — heating of sections most important for reliable cutter operation: top insert window — temperature of the cutting edge; bottom insert — temperature of the chip removal groove.

distance from the edge, as well as graphs of position, width and intensity of the diamond peak are shown in Fig. 6, *a*.

The graphs are plotted based on results of measuring the intensity of diamond line I , position of the diamond line xc ,

width of the diamond line w and grains sizes at a distance 5, 10, 15 and 20 mm from the cutter vertex.

The coating material of BK-6 milling cutter is a nanocrystalline diamond CVD film with a significant

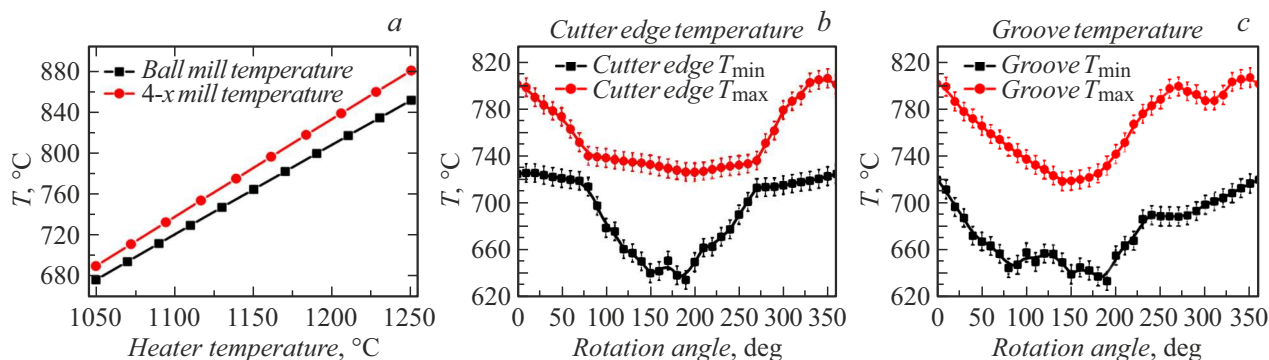


Figure 4. Results of temperature computation: *a* — computation of the heater temperature depending on the required substrate temperature; *b* — maximal and minimal heating of the cutting edge, (see Fig. 3, *c*, top insert window); *c* — minimal and maximal heating of the chip removal groove (see Fig. 3, *c*, bottom insert).

Table 2. Radii of the cutting edge of WC+6%Co cutter

Type of treatment surface	Without coating, μm	After chemical etching, μm	After sputtering tungsten, μm	After CVD diamond growth, μm
Radius	8	5	6	10

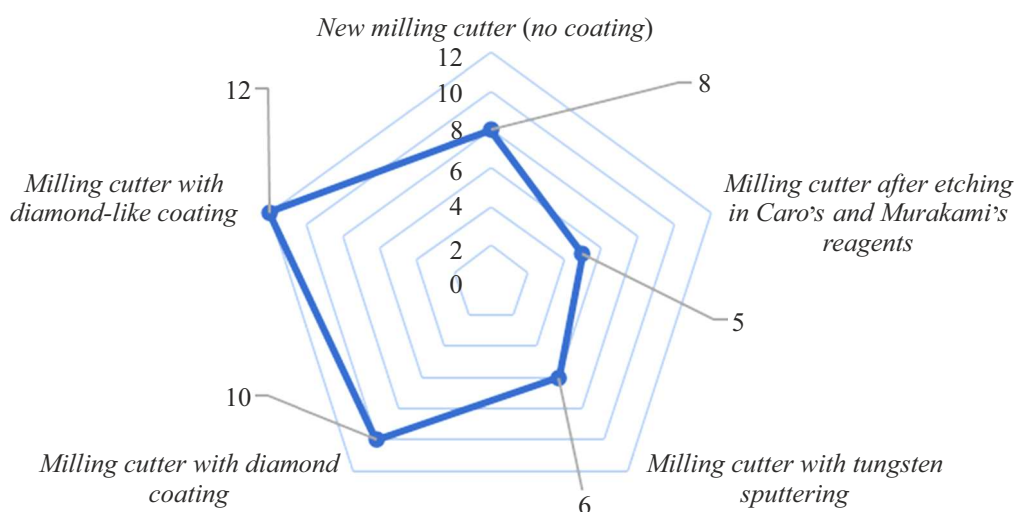


Figure 5. Diagram of radii measurements (in μm) on the cutting edge of WC+6%Co cutter with no coating and with coating.

content of disordered sp^2 -carbon and trans-polyacetylene chains C–H. As we move away from the cutter's end face the intensity of the diamond line drops by about 40%. The intensity of the diamond line I_D at $1335\text{--}1338\text{ cm}^{-1}$ changes synchronically with the growth or decrease of the size of the largest grains d_{max} : $I_D(0\text{ mm}) = 57013\text{ a.u.}$ ($d_{\text{max}} = 1.9\text{ }\mu\text{m}$)– $I_D(5\text{ mm}) = 59123\text{ a.u.}$ ($d_{\text{max}} = 2.07\text{ }\mu\text{m}$)– $I_D(10\text{ mm}) = 48627\text{ a.u.}$ ($d_{\text{max}} = 2.85\text{ }\mu\text{m}$)– $I_D(20\text{ mm}) = 30966\text{ a.u.}$ ($d_{\text{max}} = 2.9\text{ }\mu\text{m}$). This dependence is no more observed starting from 10 mm point from the end face. As can be seen, in this area there's also no dependence of the growth at full width at half maximum of the

diamond line w_D at $1335\text{--}1338\text{ cm}^{-1}$ on the decrease of size of the smallest grains d_{min} : $w_D(0\text{ mm}) = 12.6\text{ cm}^{-1}$ ($d_{\text{min}} = 80\text{ nm}$)– $w_D(5\text{ mm}) = 9.5\text{ cm}^{-1}$ ($d_{\text{min}} = 80\text{ nm}$)– $w_D(10\text{ mm}) = 9.2\text{ cm}^{-1}$ ($d_{\text{min}} = 190\text{ nm}$)– $w_D(20\text{ mm}) = 9.6\text{ cm}^{-1}$ ($d_{\text{min}} = 190\text{ nm}$). Data on the grain sizes and diamond line intensities and ordered graphite demonstrate both the uniformity of the diamond film in thickness and an increase in the proportion of microcrystalline diamond compared to nanocrystalline diamond as it moves away from the end face. Judging by position of the diamond line of Raman scattering, the diamond material experiences elastic stresses at all points, which increase as

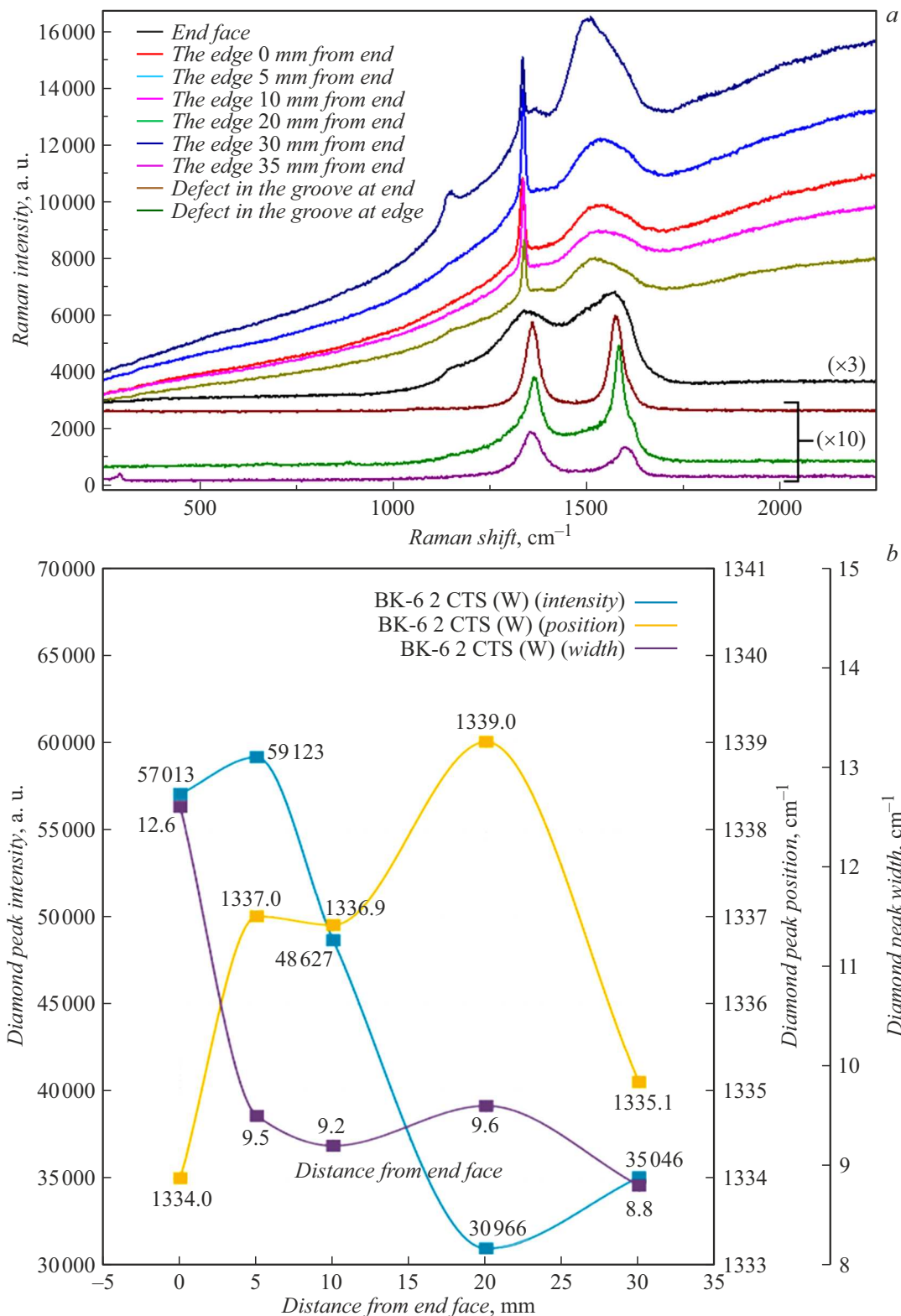


Figure 6. Results of RS MP CVD spectroscopy of MCD/NCD film on the cutter; *a* — spectra of the diamond film on WC+6%Co alloy; *b* — position, width and intensity of the diamond peak depending on the distance from the end face.

they move away from the end face from 0.7 GPa (0 mm) to 1.2 GPa (30 mm) reaching maximum at 20 mm—3.1 GPa. Interestingly, this is the only sample where the width of the

diamond peak does not increase, but decreases as it moves away from the edge. The reason for this phenomenon most likely lies in the film growth parameters. On the end face

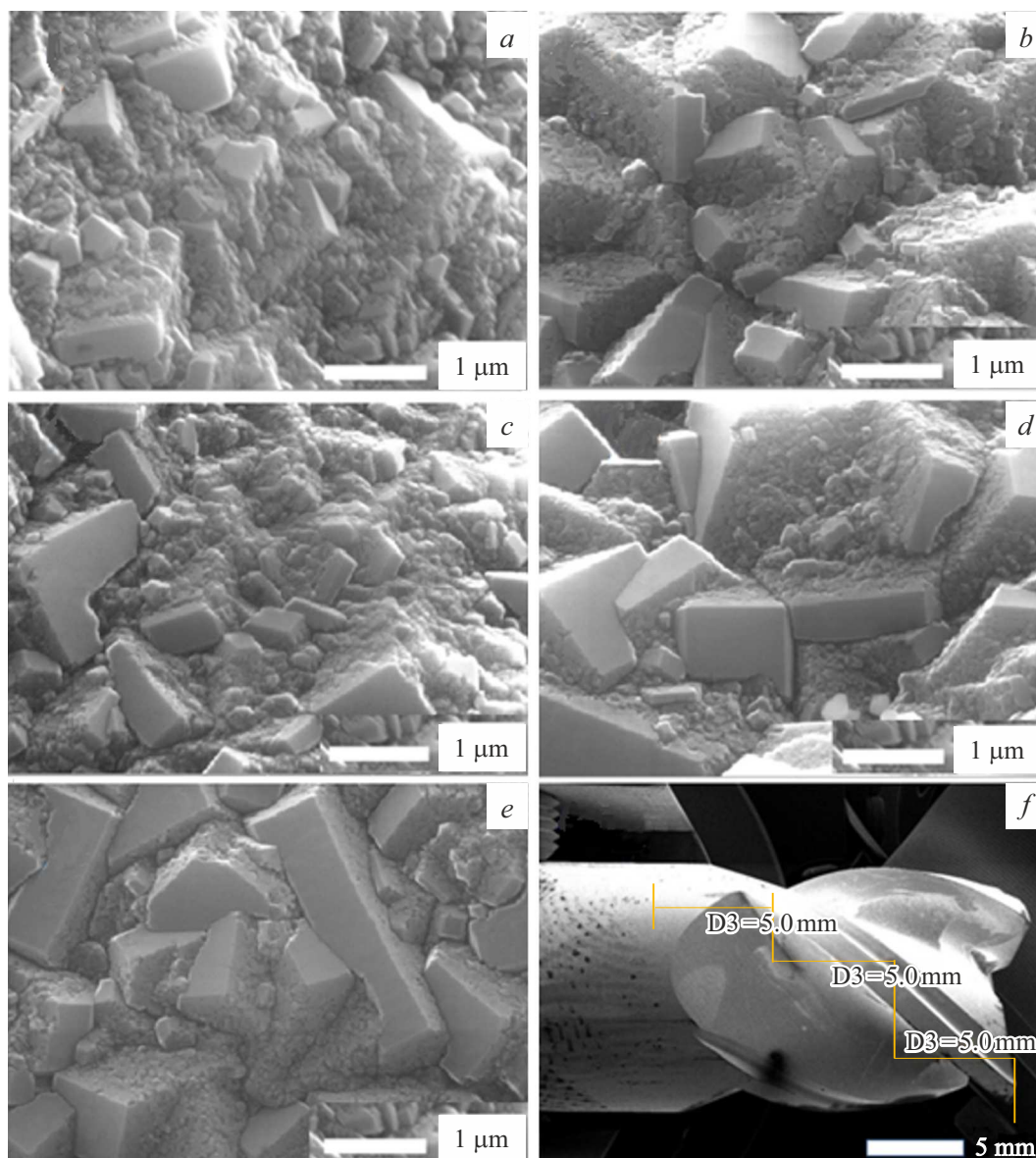


Figure 7. REM images of MCD/NCD-film microstructure, obtained during the cutter rotation: *a* — near vertex; *b* — at a distance of 5 mm from the end face; *c* — at a distance of 10 mm from the end face; *d* — at a distance of 15 mm from the end face; *e* — at a distance of 20 mm from the end face; *f* — REM scanning map with with the dimension marks on a helical line of WC+6%Co cutter.

the material represents itself a disordered sp^2 -carbon, and in the groove defects and at the cutting edge 35 mm away from the end face — a high-ordered clustered sp^2 -carbon.

2.5. Morphology of MCD/NCD diamond film surface

REM image of MCD/NCD film microstructure obtained by rotating the milling cutter, as well as at the vertex and at a distance of 5, 10, 15 and 20 mm from the end face, as well as REM scanning maps with dimensional marks on the helix are shown in Fig. 7. As can be seen, the growth of MCD/NCD diamond film during substrate rotation throughout the studied sections corresponds to the

Van der Drift competitive growth mechanism [27]. The microstructure images show how the chaotically oriented nuclei grow at different speeds, which leads to the formation of slow and fast-growing crystallites. This growth dynamics leads to an increase in the grain size of micro-crystallites with increasing film thickness [28,29].

In all cases, diamond films of uniform thickness were fabricated; when moving away from the vertex, a decrease in the proportion of nanocrystalline diamond is observed compared with the microcrystalline diamond. Diamond film on the cutter at the vertex and at a distance of 5 mm away is composed of the nanocrystalline grains with a size of about 80 nm and the microcrystalline grains with a size of about 1.9–2.1 μm , which, with a distance towards

the shank, become larger and have a size of 2.9–3.9 μm . According to their habitus, these grains have the shape of a parallelepiped or an octahedron.

Comparing the maximum grain sizes of the diamond film obtained on a cylindrical model with rotation [26], it can be seen that at a distance of 20 mm from the end face, the average grain size is $d = 62 \pm 7$ nm, at the vertex — $d = 51 \pm 7$ nm, between them — intermediate values $d = 58 \pm 7$ nm. Average grain size at a distance of 10 nm from the vertex is by 13% larger than on the end. Similarly, for the intervals 20 mm — 20% and 30 mm — 41%. In this case, the average grain sizes grow more slowly as they move away from the end face, which correlates with the local surface temperature of the sample or, in other words, with the distance from the center of plasma cloud as the diamond grows, where the maximum temperature is observed. In case of a rotating cutter sample a visible spread of habitus and grains sizes is observed, since at the cutter vertex it makes 80–1900 nm, at a distance of 5 mm — 80–2070 nm, 10 mm — 190–2850 nm, 15 mm from the end face — 110–3900 nm; and at a distance of 20 mm from the end face — 190–2900 nm. The phase is a MCD/NCD diamond film with germinated grains of microcrystalline diamond.

Conclusion

1. Based on computation of E-field of the chamber of ARDIS-100 reactor with an evanescent waveguide, a redundant area of the conducting platform was provided for the first time, which contributed to a self-consistent resonance in the field of plasma excitation and uniform field concentration around a high-dimensional substrate, starting from the active side of plasma emission and continuing along the perimeter of the milling cutter.

2. It was established that pre-treatment and CVD growth have an impact on variation of the cutting edge radius: on original WC+6%Co milling cutter — 8 μm , after etching with Co — 5 μm , with applied barrier tungsten coating — 6 μm , after growth of CVD diamond film — 10 μm .

3. The calculation established the surface temperature of the milling cutter during its rotation in a microwave reactor. Thus, on the cutting edge and in the area of the chip removal groove, which have a smaller cross-sectional area compared to a solid cylindrical model, the heating differs by no more than 60–80°C.

4. With the help of RS, it was found that the width of the diamond peak decreases as it moves away from the end of the milling cutter, which indicates an increase in the diamond film quality.

5. As seen from the RS position of the diamond line, the diamond material experiences elastic stresses at all points, which increase as they move away from the end face from 0.7 GPa (at vertex) to 1.2 GPa (at a distance of 30 mm) reaching their maximal value of 3.1 GPa at 20 mm.

6. CVD growth of MCD/NCD diamond film during rotation of the milling cutter corresponds to competitive Van der Drift growth mechanism and a lower effect of secondary nucleation with a decrease in the substrate temperature and with a constant composition of the gas mixture.

7. MCD/NCD diamond films with uniform thickness were obtained, and REM showed that with distance from the end face of the milling cutter, the microcrystalline phase proportion in the structure increases with higher grain sizes from 1900 to 3900 nm, in contrast to the nanocrystalline phase with dimensions 80–190 nm.

Acknowledgments

The authors express their thanks to M.Yu. Shevchenko and K.F. Sergeichev for participation in modeling of E-field and computations of EW UHF-reactor, respectively, as well as thanks to S.G. Ryzhkov for their help in figures design.

Funding

The study was supported by grant provided by the Russian Science Foundation № 22-19-00694.

2.6. Conflict of interest

The authors declare that they have no conflict of interest.

Appendix

Computation of the limiting size of internal radius of EW

The possibility of increasing the performance of MPA CVD is associated with the transition to simultaneous growth of several high-dimensional substrates at once. To do this, it is necessary to know the maximum diameter of EW inner radius, which ensures the relief of the „edge effect“. The possibility of improving the microwave reactor performance by placing in EW a group of high-dimensional substrates in the form of carbide cutters with an average size of 12 × 75 mm (diameter × length) is being considered.

Previously, it was experimentally found [19] that by limiting the central region of the reactor's basic conducting platform by using an axial conducting ring it is possible to make conditions of the film growth on a flat substrate more uniform, in particular, the temperature distribution on its surface becomes almost uniform. The ring's influence on the microwave field distribution is favorable for diamond growth in plasma inside the ring if its radius is less than the critical radius of the circular waveguide $R < R_c$ for a wave of E_{01} type at the operating frequency of 2.45 GHz. Critical radius of the ring was found from the expression [30]:

$$\lambda_c = \frac{2\pi}{\nu_{01}} R_c = 2.61 R_c < \lambda, \quad (\text{A1})$$

where λ — wavelength in free space, λ_c — critical wavelength of E_{01} type of wave as defined by the radius R of the waveguide, $\nu_{01} = 2.405$ — root of Bessel function.

A metal ring lying on a conductive plane is a short-circuited segment of a circular evanescent waveguide where an axisymmetric wave field of E_{01} type is excited by a vertical electrical component of the outer microwave (UHF) field. Inside the ring, the microwave field cannot propagate in the direction of the axis, since the wave propagation constant in the evanescent waveguide is $\beta = 0$, i.e. the wave phase along the height of the ring does not change, and its amplitude decays exponentially. In this case, the field decay inside the ring in the absence of plasma is determined by the formula

$$E = E_0 \exp(-\alpha \cdot z), \quad (\text{A2})$$

$$\alpha = \frac{\omega}{c} \sqrt{\frac{\lambda^2}{\lambda_c^2} - 1}, \quad (\text{A3})$$

where α — decay constant. $\omega = 2\pi c/\lambda$ — angular frequency of the field, c — light velocity. Filling the ring with dense homogeneous plasma with high temperature and effective electron collision frequency leads to an additional exponential weakening of plasma field, which in the limit $\nu_e \gg \omega$ is characterized by a depth of δ , at which the field is diminished in e times (normal skin) [31]:

$$\delta = 1/\alpha_s = \frac{c}{\omega} \sqrt{\frac{2n_c \nu_e}{n\omega}}, \quad (\text{A4})$$

where n_c — critical concentration of electrons: $n_c = \frac{m\omega^2 \epsilon_0}{e^2}$, n — concentration of plasma electrons filling the ring, e , m — charge and weight of electron, $\epsilon_0 = 8.854 \cdot 10^{-12}$ F/m — electrical constant.

Ratio of the field decay constants in the ring for the two limiting cases may be represented by parameter θ by multiplying (P3) and (P4):

$$\theta = \frac{\alpha}{\alpha_c} = \sqrt{\frac{2n_c \nu_e}{n\omega} \left(\frac{\lambda^2}{\lambda_c^2} - 1 \right)}. \quad (\text{A5})$$

At $\theta < 1$, the collisional decay mechanism (P4) dominates, and at $\theta > 1$, the field decay approaches the case of a vacuum EW filled with subcritical plasma.

Let's estimate the parameter θ inside the ring with a radius of $R = 3.5$ cm, lying on a flat base in the reactor's center for the operating frequency of 2.45 GHz (wavelength $\lambda = 12.24$ cm) for the case of diamond coating synthesis under the following conditions: 4% methane in hydrogen, flowrate of gas $Q = 500$ standard cubic centimeters per minute, pressure $p = 60$ Torr, UHF power of $P = 2.9$ kW. Rotational and gas temperatures were measured: $T_g = T_{\text{rot}} = 2600 \pm 150$ K in the central area of plasma. For estimates we additionally use the data on concentration and temperature of plasma in the discharge central area taken from computational modeling [3] for pressure of $p = 5 \cdot 10^{-2}$ bar close to the experimental value

$n_e = 10^{11}$ cm $^{-3}$. $T_e = 1.55$ eV, $T_g = 2500$ K. For the frequency of 2.45 GHz, $\omega = 1.54 \cdot 10^{10}$, critical concentration of plasma electrons $n_c = 7.45 \cdot 10^{10}$ cm $^{-3}$. The effective frequency of electronic collisions in hydrogen [2] in the hot central zone of the discharge is determined based on condition of its equilibrium with the cold peripheral zone of gas with a temperature of $T_0 \sim 300$ K at a pressure of $p = 60$ Torr through the temperatures ratio:

$$\nu_e = 7 \cdot 10^9 p \frac{T_0}{T_g}. \quad (\text{A6})$$

When we substitute the numerical values from (P1), (P3), (P4) and (P6) into expression (P5) we'll obtain parameter $\theta = 1.9$, from which it follows that inside the ring the field is weakened similar to the evanescent waveguide, while electronic collisions make additional contribution to the field decay. For instance, with the ring height of $z = 0.6$ cm at the bottom inside the ring the field strength in the absence of plasma goes down to the level of $E = E_0 \exp(-\alpha z) = \exp(-0.275)E_0 = 0.76E_0$, accordingly, over the field (power) square it is decreased to 58%. Taking into account the influence of plasma permeability, the decrease in the field strength will be even greater, since the ring is filled with plasma, which shifts the refractive index of space towards lower refractive indices n . This makes it possible to bring the inner diameter of the ring to its critical size of 90 mm, since the wavelength in plasma becomes longer than in vacuum. When high-dimensional carbide substrates with an average size of 12×75 mm (diameter \times length) are placed inside such a ring, a simultaneous growth on ten substrates at a time may occur.

References

- [1] S. Matsumoto, Y. Sato, M. Kamo, N. Setaka. Jpn. J. Appl. Phys. IOP Publishing, **21** (4A), L183 (1982).
- [2] W.A. Yarbrough, A.R. Badzian, D. Pickrell, Y. Liou, A. Inspektor. J. Cryst. Growth., **99** (1), Part 2, 1177 (1990).
- [3] Q. Liang, C.Y. Chin, J. Lai, C. Yan, Y. Meng, H. Mao, R.J. Hemley. Appl. Phys. Lett., **94** (2), 024103 (2009).
- [4] H. Toyota, S. Nomura, S. Mukasa, Y. Takahashi, S. Okuda. Diam. Relat. Mater., **19** (5), 418 (2010).
- [5] F. Silva, K. Hassouni, X. Bonnin, A. Gicquel. J. Phys. Condens. Matter., **21** (36), 364202 (2009).
- [6] J. Isberg, J. Hammersberg, E. Johansson, T. Wikström, D.J. Twitchen, A.J. Whitehead, S.E. Coe, G.A. Scarsbrook. Science, **297** (5587), 1670 (2002).
- [7] M. Kasu, M. Kubovic, A. Aleksov, N. Teofilov, R. Sauer, E. Kohn, T. Makimoto, Jpn. J. Appl. Phys. IOP Publishing, **43** (7B), L975 (2004).
- [8] J. Achard, F. Silva, A. Tallaire, X. Bonnin, G. Lombardi, K. Hassouni, A. Gicquel. J. Phys. Appl. Phys., **40** (20), 6175 (2007).
- [9] M.P. Gaukroger, P.M. Martineau, M.J. Crowder, I. Friel, S.D. Williams, D.J. Twitchen. Diam. Relat. Mater., **17** (3), 262 (2008).

- [10] F. Silva, J. Achard, X. Bonnin, O. Brinza, A. Michau, A. Secroun, K. De Corte, S. Felton, M. Newton, A. Gicquel. *Diam. Relat. Mater.*, **17** (7), 1067 (2008).
- [11] K.F. Sergejchev. *Usp. Prikl. Fiz.*, **3** (4), 342 (2015) (in Russian).
- [12] V.I. Konov, V.G. Ral'chenko, K.F. Sergejchev, V.B. Khavaev, S.K. Vartapetov, V.V. Atezhev. UHF plasma reactor, RU 2 299 929 C2, 2005.
- [13] E.A. Orozco, P. Tsygankov, Y.F. Barragan, J.A. Hernández, A. Martinez-Amariz, F.F. Parada. *Appl. Phys. A*, **129** (12), 842 (2023).
- [14] J. Zhang, J. Wang, G. Zhang, Z. Huo, Z. Huang, L. Wu. *Mater. Des.*, **237**, 112577 (2024).
- [15] A.J.S. Fernandes, V.A. Silva, J.M. Carrapichano, G.R. Dias, R.F. Silva, F.M. Costa. *Diam. Relat. Mater.*, **10** (3), 803 (2001).
- [16] A. Rifai, D. Creedon, N. Tran, M. Hejazi, D. Garrett, A.D. Greentree, E. Pirogova, A. Stacey, K. Fox. *Surf. Coat. Technol.*, **408**, 126815 (2021).
- [17] V. Sedov, A. Martyanov, A. Altakhov, A. Popovich, M. Shevchenko, S. Savin, E. Zavedeev, M. Zanaevskiy, A. Sinogeykin, V. Ralchenko, V. Konov. *Coatings*, **10** (10), 939 (2020).
- [18] H. Yamada, A. Chayahara, Y. Mokuno, Y. Horino, S. Shikata. *Diam. Relat. Mater.*, **15** (9), 1383 (2006).
- [19] E.E. Ashkihazi, V.S. Sedov, D.N. Sovyk, A.A. Khomich, A.P. Bolshakov, S.G. Ryzhkov, A.V. Khomich, D.V. Vinogradov, V.G. Ralchenko, V.I. Konov. *Diam. Relat. Mater.*, **75**, 169 (2017).
- [20] E. Ashkinazi, S. Fedorov, A. Khomich, V. Rogalin, A. Bolshakov, D. Sovyk, S. Grigoriev, V. Konov. *C (MDPI)*, **8** (4), 77 (2022).
- [21] E.E. Ashkinazi, V.Yu. Yurov, V.S. Sedov, A.P. Bolshakov, V.E. Rogalin, I.A. Antonova, V.G. Ralchenko, V.I. Konov. *Nondestructive diagnostics of diamond coatings of hard-alloy cutters* (Ekaterinburg, Russia, 2019)
- [22] V.Y. Yurov, E.E. Ashkinazi, E.V. Zavedeev, A.K. Martyanov, I.A. Antonova, V.G. Ralchenko. *Mater. Today Proc.*, **38**, 1736 (2021).
- [23] S.A. Catledge, Y.K. Vohra. *J. Appl. Phys.*, **83** (1), 198 (1998).
- [24] M.L. Terranova. *Biomedicines (MDPI)*, **10** (12), 3149 (2022).
- [25] G. Heinrich, T. Grögler, S.M. Rosiwal, R.F. Singer. *Surf. Coat. Technol.*, **94–95**, 514 (1997).
- [26] E.E. Ashkinazi, S.V. Fedorov, A.K. Martyanov, V.S. Sedov, A.F. Popovich, A.P. Bolshakov, D.N. Sovyk, S.G. Ryzhkov, A.A. Khomich, E.V. Zavedeev, A.P. Litvinov, V.Y. Yurov, S.N. Grigoriev, V.I. Konov. *Coatings (MDPI)*, **13** (7), 1156 (2023).
- [27] A. Van der Drift. *Philips Res Rep.*, **22** (3), 267 (1967).
- [28] V.G. Ralchenko, E. Pleuler, F.X. Lu, D.N. Sovyk, A.P. Bolshakov, S.B. Guo, W.Z. Tang, I.V. Gontar, A.A. Khomich, E.V. Zavedeev, V.I. Konov. *Diam. Relat. Mater.*, **23**, 172 (2012).
- [29] V. Sedov, A. Martyanov, S. Savin, E. Zavedeev, O. Kudryavtsev, H. Bland, S. Mandal, O. Williams, V. Ralchenko, V. Konov. *Diam. Relat. Mater.*, **114**, 108333 (2021).
- [30] I.V. Lebedev. *Tekhnika i pribory SVCH* (Vysshaya shkola, Moskva, 1970), p. 1. (in Russian).
- [31] V.E. Golant. *Microwave method of plasma investigation* (Nauka, M., 1968) (in Russian)

Translated by T.Zorina